Energy-flux pattern in the Goos-Hänchen effect

H. M. Lai,* C. W. Kwok, Y. W. Loo, and B. Y. Xu
Department of Physics, The Chinese University of Hong Kong, Shatin, Hong Kong, China
(Received 16 May 2000)

The (two-dimensional) wave beam fields and the associated energy flux in the Goos-Hänchen effect are studied analytically and numerically. In particular, the time-averaged Poynting vector and its flux lines around the interface are calculated for both states of wave polarization, irrespective of a positive shift (the usual one) or a negative shift of the reflected beam. For a given transverse field profile of the incident beam, the flux lines associated with the evanescent waves for the two cases of shift are shown to have the same shape yet to take opposite directions; they are parabolas if the profile is Gaussian. The flux lines in the first medium are shown to connect to those in the second medium on the two sides of the interface. In the case of positive shift, the whole flux pattern expectedly shows the supply of energy from the incident beam to the evanescent wave on one side and the return of energy on the other side to the reflected beam. In the case of negative shift, on the other hand, the flux lines nearby the interface form loops, in addition to the expected incoming-outgoing flux pattern in the remaining region.

PACS number(s): 42.25.Gy, 01.55.+b, 41.85.−p

I. INTRODUCTION

The Goos-Hänchen (GH) effect, which refers to the lateral shift of a totally reflected wave beam from the path usually expected from geometrical optics, was discovered by Goos and Hänchen and theoretically explained by Artmann in the late 1940s [1,2]. It has since then been further studied theoretically (see, for example, [3–9]) and experimentally (see, for example, [10–14]). Its consideration has been extended to cases involving multilayered structures (see, for example, [15]), absorptive media (see, for example, [16–18]), and nonlinearities (see, for example, [19]); its relevance to optical waveguides (see, for example, [20]) and near-field scanning optical microscopy [(NSOM), see, for example, [21,22]] has also been investigated. Moreover, attention has been drawn to the existence of a negative GH shift in some circumstances [15–18,23].

The energy flux around the interface between the two media in the effect is important in the understanding of the phenomenon, especially in the case of a negative shift. Furthermore, knowledge of the fields, the evanescent wave in particular, is useful in applications related to NSOM and the attenuated total reflection spectroscopy. Yet so far there has been little satisfactory calculation of these quantities. Lotsch [4] has calculated the fields and the time-averaged Poynting vectors using a scheme which starts by expressing every field quantity (including the incident one) as a sum of a dominant term (or ''amplitude'' term) and a subdominant term (or ''amplitude-derivative'' term), each with some coefficients to be determined by boundary conditions. His results are complicated and do not readily give the energy flux lines in the whole region even for simple cases, e.g., the case of a Gaussian beam. Moreover, his result on the shift agrees closer with Renard's [3] than with Artmann's [2], which has led to controversies [7,9,12]. There is, therefore, a need to reconsider the problem. This is exactly the purpose of this paper. Our method is different from but simpler than Lotsch's, and leads to results in complete agreement with Artmann's and many others. It starts with the (spatial) Fourier integral of the monochromatic (i.e., single-frequency) incident beam field, which is essentially a linear superposition of sinusoidal plane waves with wave vectors of *different* directions but of the *same* magnitude. This method has been widely used to find the shift of the reflected beam [5–9]. Here we use it to calculate the explicit field variation in the two media. The well-known reflection and transmission coefficients for each sinusoidal plane wave can be readily used under the integral to yield the reflected beam field and the ''transmitted'' (or ''refracted'') beam field, hence the Poynting vectors and flux lines in the two media. The boundary conditions and the energy conservation are automatically guaranteed. Both states of wave polarization (TE or *s* state and TM or *p* state) as well as both directions (positive and negative) of shift are considered in one shot. Like Lotsch's, our consideration is restricted to two-dimensional fields and assumes a small divergence angle of the beam, meaning that the wavelength is much smaller than the beam width, which is assumed to be of the order of the transverse scale length.

In Sec. II general consideration is given, together with the setting up of notations and necessary formulas to be used later. In Sec. III we evaluate the fields in the lowest approximation of a good collimated wave beam. Not only the shifted reflected beam field is calculated, a properly shifted transmitted beam field (i.e., the evanescent wave field) is also obtained. In Sec. IV the time-averaged Poynting vector in the two media is calculated and the energy flux lines are obtained and plotted under the same approximation. Both the *s* state and the *p* state of polarization, and both the positive shift case (the usual one) and the negative shift case, are considered along the calculation. The negative shift case, which corresponds to a backward energy flow associated with the TM-state evanescent waves in the second medium of the negative dielectric constant (or permittivity), is stressed; its energy flow pattern in the region around the interface is particularly shown from our quantitative results.

*Email address: hmlai@cuhk.edu.hk

Only nonmagnetic media without spatial dispersion are considered, meaning that the Poynting vector gives the energy flux density. Furthermore, the cgs Gaussian unit system is used throughout the paper.

II. GENERAL CONSIDERATION

Consider two semi-infinite homogeneous media separated by a flat interface which will be defined as the xy plane. Let there be an incident plane-polarized monochromatic wave of the form $\exp(i\mathbf{k}\cdot\mathbf{r}-i\omega t)$ in the lower ($z<0$) medium (hereafter referred to as the first medium) with the wave vector $\mathbf{k}$ lying in the xz plane and making an angle θ with the z axis. The wave is either in the TE state or in the TM state. At the frequency ω, both media are assumed to be nonabsorptive, with the first medium having a real positive dielectric constant ϵ_1 and the second a real dielectric constant ϵ_2, which can be either positive or negative. As an example for the latter case, we have in mind a cold field-free plasma at ω below the plasma frequency.

As is well known, the incident wave is accompanied by a reflected wave and a ''transmitted'' wave of the same form with the following reflection and transmission coefficients:

$$r=\frac{k_z-\mu k_z^{(t)}}{k_z+\mu k_z^{(t)}} \quad \text{and} \quad t=\frac{2k_z}{k_z+\mu k_z^{(t)}}, \tag{1}$$

where k_z is the z component of the wave vector of the incident wave and $k_z^{(t)}$ is that of the transmitted wave, both satisfying their respective dispersion relations:

$$k_z^2=\epsilon_1\omega^2/c^2-k_x^2 \quad \text{and} \quad k_z^{(t)2}=\epsilon_2\omega^2/c^2-k_x^2 \tag{2}$$

in their corresponding media, with k_x being the x component of the wave vector. Note that in Eq. (1) μ is an index for the state of wave polarization, having the value

$$\mu=1 \quad \text{or} \quad \mu=\epsilon_1/\epsilon_2 \tag{3}$$

for the TE state or the TM state, respectively. Note also that, for the former case where the electric field is along the y direction, the coefficients r and t are the ratios of the electric fields while, for the latter case where the magnetic field is along the y direction, they refer to the ratios of the magnetic fields (see also [9]). Furthermore, $k_x=k\ \sin\theta$ and $k_z=k\ \cos\theta$, where k, being equal to $\sqrt{\epsilon_1}\ \omega/c$, is the magnitude of the wave vector in the first medium.

In this paper we shall restrict to the following two cases: (a) the usual total internal reflection where $\epsilon_1>\epsilon_2\geqslant 1$ and $\theta>\theta_c$, the critical angle defined by $\sin^{-1}\sqrt{\epsilon_2/\epsilon_1}$; (b) the total reflection with a negative dielectric constant of the second medium, i.e., $\epsilon_2<0<\epsilon_1$. They both give the well-known evanescent waves in the second medium with the same real k_x and a purely imaginary $k_z^{(t)}$, which is often written as

$$k_z^{(t)}=i\kappa \quad \text{with} \quad \kappa\equiv\sqrt{k_x^2-\epsilon_2\omega^2/c^2}>0, \tag{4}$$

where $1/\kappa$ is the ''skin depth'' of the field in the second medium [24]. The two coefficients r and t can now be simplified to

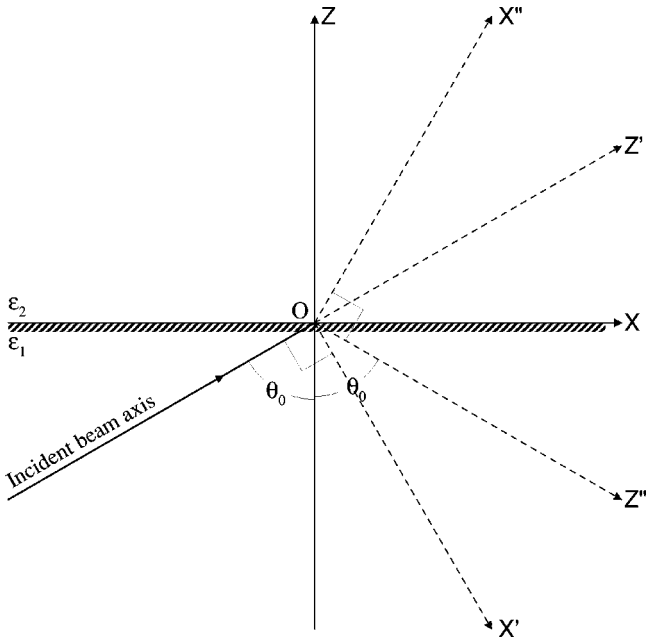

FIG. 1. The original XYZ coordinate system, the incident $X'YZ'$ coordinate system, and the reflection (left-handed) $X''YZ''$ coordinate system, all with the same Y axis directed into the plane of the figure and the same origin O. Note that the XY plane separates the two media of ϵ_1 and ϵ_2.

$$r=\exp(-i\phi) \quad \text{and} \quad t=|t|\ \exp(-i\phi/2), \tag{5}$$

where

$$\phi/2\equiv\tan^{-1}(\mu\kappa/k_z) \quad \text{and} \quad |t|=2k_z/\sqrt{k_z^2+\mu^2\kappa^2}. \tag{6}$$

Here we note that the phase in t is exactly half of that in r.

We now consider a monochromatic wave *beam* incident from below upon the interface with the beam line of maximum intensity (hereafter referred to as the beam axis) lying in the xz plane and passing through the origin. The beam is two-dimensional so that every field quantity is independent of the y coordinate, and it is either in the TE state or in the TM state. To facilitate the calculation, we introduce, as shown in Fig. 1, the incident $X'YZ'$ coordinate system and the reflection $X''YZ''$ coordinate system in addition to the original XYZ coordinate system, all with the same y axis (directed into the plane of the figure) and the same origin O. The z' axis, which makes an angle θ_0 with the z axis, coincides with the incident beam axis while the z'' axis coincides with the reflection beam axis if there is no GH shift. Note that the x'' axis is so chosen that a plane wave of positive k_x' gives the reflected wave again with a positive k_x''; hence $X''YZ''$ is a left-hand coordinate system.

Being monochromatic, the field always depends on time through the factor $\exp(-i\omega t)$. Omitting this temporal factor, the field (electric for the TE state and magnetic for the TM state) of the *incident* beam, being a linear superposition of plane sinusoidal waves, can in general be written as

$$\mathbf{F}^{(i)}(x',z')=\int_{-k}^{k} G(k_x')\ \exp(ik_x'x' + ik_z'z')dk_x'\ \hat{\mathbf{y}} \quad \text{for} \quad z\leqslant 0 \tag{7}$$

in the incident coordinate system, where $\hat{\mathbf{y}}$ is the unit vector along the y axis and $k_z' = \sqrt{k^2 - k_x'^2}$. Since we already know how each incident sinusoidal wave is accompanied by a reflected sinusoidal wave and a transmitted sinusoidal wave, obviously the accompanied reflected and transmitted beam fields are, respectively, given by

$$\mathbf{F}^{(r)}(x'',z'') = \int_{-k}^{k} r(k_x')G(k_x') \ \exp(ik_x'x'' + ik_z'z'')dk_x' \ \hat{\mathbf{y}} \quad \text{for} \quad z \leqslant 0 \tag{8}$$

in the reflection coordinate system, and

$$\mathbf{F}^{(t)}(x,z) = \int_{-k}^{k} t(k_x')G(k_x') \ \exp(ik_x x - \kappa z)dk_x' \ \hat{\mathbf{y}} \quad \text{for} \quad z \geqslant 0 \tag{9}$$

in the original coordinate system, where r, t, and κ, given respectively by Eqs. (1) and (4), are functions of k_x' through the following transformations:

$$k_x = k_x' \cos\theta_0 + k_z' \sin\theta_0, \quad k_z = -k_x' \sin\theta_0 + k_z' \cos\theta_0, \tag{10}$$

with k_z' being a function of k_x'. Note that, in Eq. (8), we have made use of the fact that a wave of wave vector (k_x', k_z') is reflected into a wave with exactly the same values of (k_x'', k_z''). Note also that the field in Eq. (9) is simply a linear superposition of the evanescent waves of different k_x's.

To find the energy flux, the well-known expression for the time-averaged Poynting vector, given by

$$\mathbf{S} = \frac{c}{8\pi} \ \text{Re} \ [\mathbf{E} \times \mathbf{B}^*], \tag{11}$$

with Re meaning ''the real part of,'' turns out to be

$$\mathbf{S} = \frac{c^2}{8\pi\omega} \ \text{Re} \ [i\mathbf{F} \times (\boldsymbol{\nabla} \times \mathbf{F})^*] \tag{12}$$

for the TE state where $\mathbf{F}$ is the electric field (hence $-ic\boldsymbol{\nabla} \times \mathbf{F}/\omega$ is the magnetic field), and

$$\mathbf{S} = \frac{c^2}{8\pi\omega\epsilon} \ \text{Re} \ [i\mathbf{F} \times (\boldsymbol{\nabla} \times \mathbf{F})^*] \tag{13}$$

for the TM state where $\boldsymbol{F}$ is the magnetic field (hence $ic\boldsymbol{\nabla} \times \mathbf{F}/\epsilon\omega$ is the electric field). Therefore, in either case, we need only to consider the same quantity $\mathbf{F} \times (\boldsymbol{\nabla} \times \mathbf{F})^*$.

At this point, it is worth pointing out that, by definition, the (instantaneous) Poynting vector for the TE state is continuous across the interface while, for the TM state, ϵS_x and S_z are continuous across the interface. These boundary conditions are useful in evaluating the energy fluxes in the two media. Of course, the continuity of the normal component in both cases is required by the conservation law.

Furthermore, we want to call attention to the fact that, for the total reflection of an incident sinusoidal *plane* wave in the TM state (i.e., p state), $\boldsymbol{\nabla} \times \mathbf{F} = i\mathbf{k}^{(t)} \times \mathbf{F}^{(t)}$ in the second medium and the associated time-averaged Poynting vector in Eq. (13) becomes

$$\mathbf{S} = \frac{c^2 k_x}{8\pi\omega\epsilon_2} |\mathbf{F}^{(t)}|^2 \ \hat{\mathbf{x}}. \tag{14}$$

As the energy flux density of the evanescent wave, it only has an x component as expected. Yet it also implies a backward energy flow if ϵ_2 is negative. This is important in the understanding of the negative shift.

III. CALCULATION OF FIELDS

We consider a good collimated incident beam. By this we mean the divergence angle of the beam is very small such that the integrand $G(k_x')$ in Eq. (7) is substantial only around $k_x' = 0$ with a (spectrum) width $\triangle k_x'$ much smaller than the integration limit, i.e.,

$$\triangle k_x'/k \ll 1 \quad \text{or} \quad kW \gg 1, \tag{15}$$

where we have introduced the beam width W (or the scale length of the transverse field) and we have assumed it to be of the order of the inverse of the (spectrum) width. For a good laser beam of millimeter width, kW is as large as 10^4. A lot of beam properties can be studied analytically with Eq. (7) through this assumption by expanding k_z' in terms of k_x' and by setting the integration limits essentially to infinities. For example, keeping the expansion to the second order and taking

$$G(k_x') = \sigma F_0 \exp(-k_x'^2\sigma^2/2), \tag{16}$$

Eq. (7) gives the following well-known (two-dimensional) Gaussian beam propagating along the z' axis and of a minimum root-mean-square width σ of the *field* distribution at $z' = 0$ [25,26]:

$$\mathbf{F}^{(i)}(x',z') = F_0 \ \sqrt{\frac{\sigma}{\sigma_{z'}}} \exp\left(-\frac{x'^2}{2\sigma_{z'}^2}\right) \ e^{i\Psi(x',z')} \ e^{ikz'} \ \hat{\mathbf{y}}, \tag{17}$$

where

$$\sigma_{z'} \equiv \sqrt{\sigma^2 + \frac{z'^2}{k^2\sigma^2}} \tag{18}$$

is the root-mean-square beam width at z', and

$$\Psi(x',z') \equiv \frac{z'x'^2}{2k\sigma^2\sigma_{z'}^2} - \frac{1}{2} \ \tan^{-1}\frac{z'}{k\sigma^2} \tag{19}$$

is the additional phase factor.

For our purpose in this paper we shall neglect the second- (and higher-) order terms in the expansion of k_z' in Eq. (7). This means

$$|z'|/kW^2 \ll 1. \tag{20}$$

We shall henceforth restrict our interest to the region not too far from the origin or, noting that kW^2 is essentially the

Rayleigh range defined for a wave beam [25], to the region well within the Rayleigh range from the focus. Consequently, the incident beam in Eq. (7) readily reduces to

$$\mathbf{F}^{(i)}(x',z')=T(x')e^{ikz'}\ \hat{\mathbf{y}}, \tag{21}$$

where

$$T(v)\equiv\int_{-\infty}^{\infty}G(k_x')\ \exp(ik_x'v)dk_x' \tag{22}$$

is the transverse profile of the incident beam field. This is the lowest-order approximation of a good collimated beam.

The reflected field can be obtained in a similar fashion with the additional expansion of the phase in Eq. (5) in terms of k_x' to the first order. The result has essentially been obtained before [8,9]. It is, from Eq. (8),

$$\mathbf{F}^{(r)}(x'',z'')=e^{-i\phi_0}\ T(x''-D)e^{ikz''}\ \hat{\mathbf{y}}, \tag{23}$$

a field shifted from the z'' axis (in the reflection coordinate system as shown in Fig. 1) by a distance D, where

$$D\equiv\frac{d\phi}{dk_x'}=\frac{d\phi}{kd\theta}, \tag{24}$$

evaluated at $k_x'=0$ or $\theta=\theta_0$, is the well-known expression for the GH shift first obtained by Artmann [2] through the method of stationary phase. The explicit form is, in our notation,

$$D=\frac{2\mu\ (1-\epsilon_2/\epsilon_1)\ \sin\theta_0}{\kappa_0\ (\cos^2\theta_0+\mu^2\kappa_0^2/k^2)}, \tag{25}$$

where

$$\kappa_0=k\sqrt{\sin^2\theta_0-\epsilon_2/\epsilon_1}. \tag{26}$$

Three remarks are in order. First, for the usual case of total internal reflection, D blows up at the critical angle but the expression is good as long as $\theta_0-\theta_c>1/kW$. The shift around and off the critical angle has been obtained in [9]. When compared to a wavelength, it is large around the critical angle but otherwise it is of the same order of magnitude; nevertheless, it is always small compared to the beam width. Second, the method of stationary phase is not necessary in obtaining the result (see [8,9]); in fact, the reflected field as expressed by Eq. (23) is good in the region around the interface, where the method of stationary phase fails to apply. Third, the shift in Eq. (25) is good for the two states of polarization ($\mu=1$ for the TE state and $\mu=\epsilon_1/\epsilon_2$ for the TM state) and for the two directions of shift. In particular, the shift D has the same sign as μ, which is negative for a negative ϵ_2 when the beam field is in the TM state (i.e., the p state of wave polarization).

To obtain the transmitted field in Eq. (9) under the same approximation is a bit more involved. In addition to the expansion of the phase of t in a similar fashion, we have to expand k_x, $|t|$, and κ to first order in k_x'. The first is readily obtained from Eq. (10) and the last two have the following results in a straightforward way:

$$|t|=|t|_0(1-\alpha k_x') \quad \text{and} \quad \kappa=\kappa_0+\beta k_x', \tag{27}$$

where

$$|t|_0=2\cos\frac{\phi_0}{2}=\frac{2\cos\theta_0}{\sqrt{\cos^2\theta_0+\mu^2\kappa_0^2/k^2}} \tag{28}$$

and

$$\alpha=\frac{D}{2}\tan\frac{\phi_0}{2}=\frac{\mu\kappa_0 D}{2k\cos\theta_0}, \quad \beta=k\sin\theta_0\cos\theta_0/\kappa_0. \tag{29}$$

We now substitute all these expansions in Eq. (9) in addition to that for the phase. The result is

$$\mathbf{F}^{(t)}(x,z)=|t|_0\ \ e^{-\kappa_0 z+i(kx\sin\theta_0-\phi_0/2)}[T(\bar{x}\cos\theta_0)+i(\alpha+\beta z)\dot{T}(\bar{x}\cos\theta_0)]\ \hat{\mathbf{y}} \tag{30}$$

for $z\geqslant 0$, where we have assumed $z\ll W$ so that $e^{-\beta k_x' z}=1-\beta k_x' z$ is valid, and we have also introduced the shifted coordinate variable along the x direction

$$\bar{x}\equiv x-\frac{D}{2\cos\theta_0} \tag{31}$$

and the spatial derivative

$$\dot{T}(v)\equiv\frac{dT(v)}{dv}=\int_{-\infty}^{\infty}ik_x'G(k_x')\exp(ik_x'v)dk_x'. \tag{32}$$

We see that in Eq. (30) the argument of T has a ''coordinate change'' of $D/2\cos\theta_0$ along the x axis, indicating a shift of the ''transmitted'' field strength corresponding to the shift of the reflected beam field. The 1/2 factor is due to the phase in t just half as much as that in r, as obvious from Eq. (5). Furthermore, we want to point out that the transmitted field in such a coordinate-shifted form as given by Eq. (30) has not been obtained before.

With the $\mathbf{F}$'s in Eqs. (21), (23), and (30), the corresponding $\nabla\times\mathbf{F}$'s are simply

$$\nabla\times\mathbf{F}^{(i)}=\left[-ik\ \hat{\mathbf{x}}'+\frac{\dot{T}(x')}{T(x')}\ \hat{\mathbf{z}}'\right]F^{(i)}, \tag{33}$$

$$\nabla\times\mathbf{F}^{(r)}=\left[ik\ \hat{\mathbf{x}}''-\frac{\dot{T}(x''-D)}{T(x''-D)}\ \hat{\mathbf{z}}''\right]F^{(r)}, \tag{34}$$

and

$$\nabla\times\mathbf{F}^{(t)}=\left[\kappa_0-i\beta\frac{\dot{T}(\bar{x}\cos\theta_0)}{T(\bar{x}\cos\theta_0)}\right]F^{(t)}\ \hat{\mathbf{x}}+\left[ik\sin\theta_0+\frac{\dot{T}(\bar{x}\cos\theta_0)}{T(\bar{x}\cos\theta_0)}\right]F^{(t)}\ \hat{\mathbf{z}}, \tag{35}$$

where $F^{(i)}$, $F^{(r)}$, and $F^{(t)}$ are the y components of the incident, reflected, and transmitted $\mathbf{F}$ fields, respectively, terms

of double derivatives of T have been ignored, and terms with a product of $\dot{T}$'s are understood to be discarded.

Two points are to be noted. First, the fields obtained in this section can be easily expressed in terms of the original coordinate system through the following transformations between the coordinate unit vectors:

$$\hat{\mathbf{x}}' = \hat{\mathbf{x}}\cos\theta_0 - \hat{\mathbf{z}}\sin\theta_0, \quad \hat{\mathbf{z}}' = \hat{\mathbf{x}}\sin\theta_0 + \hat{\mathbf{z}}\cos\theta_0, \tag{36}$$

$$\hat{\mathbf{x}}'' = \hat{\mathbf{x}}\cos\theta_0 + \hat{\mathbf{z}}\sin\theta_0, \quad \hat{\mathbf{z}}'' = \hat{\mathbf{x}}\sin\theta_0 - \hat{\mathbf{z}}\cos\theta_0,$$

hence the relation of (x',z') or (x'',z'') to (x,z) is also obvious.

Second, these fields (electric or magnetic) satisfy their respective boundary conditions (i.e., the continuity of the tangential electric field and the tangential magnetic field across the interface at $z=0$) for both the TE state and the TM state. This can be shown if we note the relations $x' = \bar{x}\cos\theta_0 + D/2$ and $x'' - D = \bar{x}\cos\theta_0 - D/2$, then expand the T functions in Eqs. (21) and (23) [or Eqs. (33) and (34) for the other field] around $\bar{x}\cos\theta_0$ to first order in D, and compare with the field in Eq. (30) [or Eq. (35) for the other field] in the second medium, using the relations in Eqs. (25), (28), and (29). Though this is expected, it is the *shifted* transmitted field that makes the boundary conditions nicely satisfied.

IV. CALCULATION OF ENERGY FLUX AND FLUX LINES

We now use Eqs. (12) and (13) to find the time-averaged Poynting vector or the energy-flux density in the two media. It turns out that the calculation simplifies a lot and the physics is more transparent if the transverse profile $T(x')$ of the incident beam field in Eq. (21) is real. This is what we will assume in the following.

A. First medium ($z \leqslant 0$)

With the assumption of a real $T(x')$, the incident and the reflection beams, treated separately, are easily shown to have unidirectional flux lines. The time-averaged Poynting vector corresponding to the *total* field is thus given by

$$\mathbf{S} = \mathbf{S}^{(i)} + \mathbf{S}^{(r)} + \mathbf{S}^{(m)}, \tag{37}$$

where, except for the factor $c^2/8\pi\omega$ for the TE case,

$$\mathbf{S}^{(i)} = k[T(x')]^2 \ \hat{\mathbf{z}}' \quad \text{and} \quad \mathbf{S}^{(r)} = k[T(x''-D)]^2 \ \hat{\mathbf{z}}'' \tag{38}$$

are, respectively, the incident beam energy flux and the reflected beam energy flux considered separately, and, with $\Phi \equiv 2kz\cos\theta_0 + \phi_0$,

$$\mathbf{S}^{(m)} = 2kT(x')T(x''-D)\sin\theta_0\cos\Phi \ \hat{\mathbf{x}} + [\dot{T}(x') \times T(x''-D)\hat{\mathbf{x}}' - T(x')\dot{T}(x''-D)\hat{\mathbf{x}}'']\sin\Phi \tag{39}$$

is the mixed-product term or the interference term after some manipulations. Note that, in the derivation, second-order terms have been thrown away. The result for the TM state is the same except for an additional factor ϵ_1, the dielectric constant of the first medium, in the denominator. This is obvious from Eq. (13) versus Eq. (12).

Because of the shift of the reflected beam as shown by Eq. (38), it is natural to introduce the *shifted* coordinate system $(\bar{x},\bar{z})$, where $\bar{x}$ is defined by Eq. (31) and $\bar{z}$ by

$$\bar{z} \equiv z - \frac{D}{2\sin\theta_0}. \tag{40}$$

This is simply a coordinate system parallelly displaced from the original system with the origin $\bar{O}$ now being the intersection of the incident beam axis and the (actual) reflected beam axis. Obviously,

$$x' = \bar{x}\cos\theta_0 - \bar{z}\sin\theta_0 \quad \text{and} \quad x'' - D = \bar{x}\cos\theta_0 + \bar{z}\sin\theta_0. \tag{41}$$

Inside the first medium, the situation is therefore like two crisscrossing unidirectional beams, one pointing towards and the other pointing away from the new origin $\bar{O}$. Note that the new origin, though expectedly located in the second medium (or more exactly in the first quadrant of the original coordinate system) for the case of positive shift, is nevertheless located inside the *first* medium (or more exactly in the third quadrant of the original coordinate system) for the case of negative shift.

We now consider the flux lines from the well-known formula

$$d\bar{z}/d\bar{x} = S_z/S_x, \tag{42}$$

where the two components of the Poynting vector, in terms of $(\bar{x},\bar{z})$, are obtainable from Eqs. (38) and (39), with the aid of Eqs. (36) and (41). To find out the flux lines explicitly, let us assume a Gaussian profile, i.e.,

$$T(v) = \exp(-v^2/2\sigma^2), \tag{43}$$

where the coefficient has been ignored without loss of generality. We then get

$$S_x = 2kT(x')T(x''-D)\sin\theta_0 \times \left[\cosh\frac{\bar{x}\bar{z}\sin 2\theta_0}{\sigma^2} + \cos\Phi + \frac{\bar{z}\cos\theta_0\sin\Phi}{k\sigma^2}\right] \tag{44}$$

and

$$S_z = 2kT(x')T(x''-D)\cos\theta_0 \times \left[\sinh\frac{\bar{x}\bar{z}\sin 2\theta_0}{\sigma^2} + \frac{\bar{x}\sin\theta_0\sin\Phi}{k\sigma^2}\right] \tag{45}$$

in a straightforward way, where the terms involving $\sin\Phi$ and $\cos\Phi$ are due to interference. We see that outside the overlapped region of the two beams where $\bar{x}\bar{z}/\sigma^2 \gg 1$, the two hyperbolic functions dominate and Eq. (42) readily reduces to

$$d\bar{z}/d\bar{x} \to \pm \cot\theta_0 \quad \text{for} \quad \bar{x}\bar{z} \to \pm\infty, \tag{46}$$

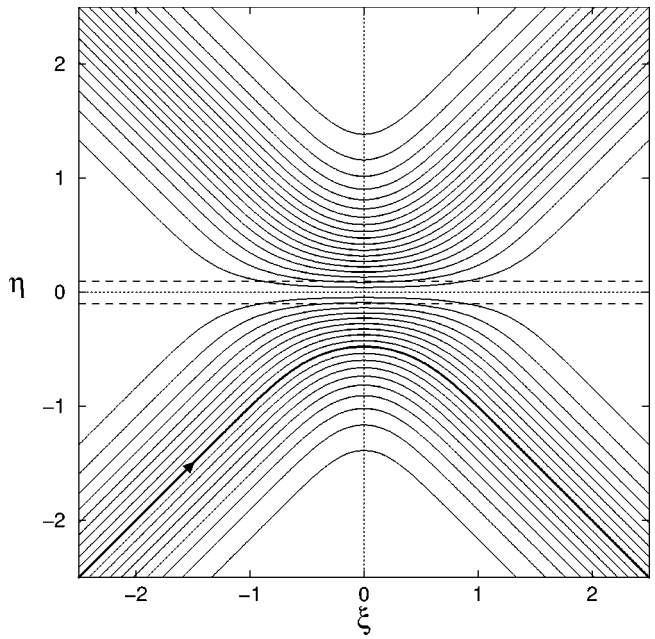

FIG. 2. Solution of Eq. (47) for a Gaussian beam. The two dashed lines at $\eta = D/(2\sigma) = -0.1$ and 0.1 indicate the position of the interface for the case of positive shift and the case of negative shift, respectively. The bold line on the lower left coincides with the incident beam axis.

which clearly refers to the expected straight flux lines of the incident beam and the reflected beam, respectively, at large distance.

To include the overlapped region, the simplest is to ignore the interference. The flux lines in such a case are in fact those corresponding to the Poynting vector spatially averaged over a wavelength along the z direction. They obey the following nonlinear equation

$$d\eta/d\xi = \tanh 2\xi\eta, \tag{47}$$

where the dimensionless coordinates

$$\xi \equiv \overline{x}\cos\theta_0/\sigma \quad \text{and} \quad \eta \equiv \overline{z}\sin\theta_0/\sigma \tag{48}$$

have been introduced. To our knowledge, the equation has no closed-form solution. Yet it is invariant under the change of sign of any one of the two variables. So the general solutions must be even in ξ and η. They are numerically obtained and shown in Fig. 2, where the cross-sectional density of the flux lines tells the intensity of the Gaussian beam, and the two perpendicular dotted lines (i.e., the $\xi\eta$-coordinate lines) intersect at $\overline{O}$, which is not marked in the figure for neatness. The whole graph gives the energy-flux pattern of the two crisscrossing wave beams, one with the field in Eq. (21) and the other with the field in Eq. (23), when the interference is ignored. For the present case of the GH effect, only the flux lines in the region $\eta < -D/2\sigma$ (i.e., the first medium where $z<0$) are physically meaningful, and they will connect to those in the second medium to be found in Sec, IV B. Since D can be either positive or negative, we show in the figure two horizontal dashed lines, the upper one indicating the position of the interface in the case of negative shift and the lower one in the case of positive shift.

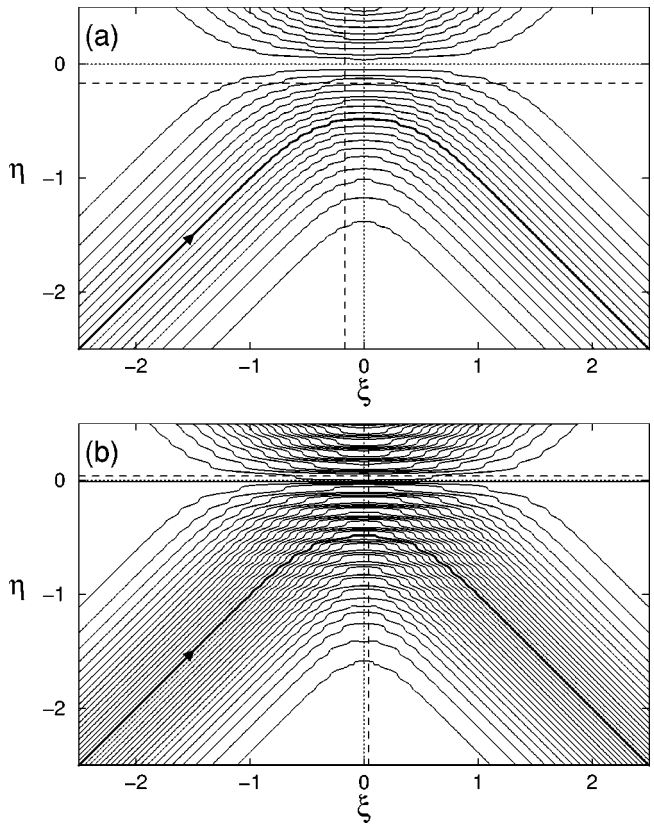

FIG. 3. Solutions of Eq. (49) for a gaussian beam in the TM state. (a) A positive-shift case where $\epsilon_1 = 2.1$, $\epsilon_2 = 1$, $\theta_0 = 45°$, $k\sigma = 50$, and (b) a negative-shift case where $\epsilon_1 = 1$, $\epsilon_2 = -0.15$, $\theta_0 = 18°$, and $k\sigma = 10$. In either figure, only the pattern in the region below the horizontal dashed line is physically meaningful, and the bold line on the lower left coincides with the incident beam axis. Note that $D/2\sigma = 0.1666$ and $\theta_c = 43.64°$ in case (a), and $D/2\sigma = -0.04047$ in case (b).

Including the interference terms, we have the following modified equation:

$$\frac{d\eta}{d\xi} = \frac{\sinh 2\xi\eta + \xi\tan\theta_0 \sin\Phi/k\sigma}{\cosh 2\xi\eta + \cos\Phi + \eta\cot\theta_0\sin\Phi/k\sigma}, \tag{49}$$

where $\Phi = (2k\sigma\eta + kD)\cot\theta_0 + \phi_0$. The symmetry in η is broken while that in ξ remains. Figure 3(a) gives the flux lines in the TM state for a case of positive shift, where $\epsilon_1 = 2.1$, $\epsilon_2 = 1$, $\theta_0 = 45°$, and $k\sigma = 50$ have been taken, implying $D/2\sigma = 0.1666$ and $\theta_c = 43.64°$. To save space, we have not shown the flux pattern for the TE state, which is similar to that for the TM state. Figure 3(b) gives the flux lines in the TM state for a case of negative shift, where $\epsilon_1 = 1$, $\epsilon_2 = -0.15$, $\theta_0 = 18°$, and $k\sigma = 10$, implying $D/2\sigma = -0.040\,47$. In both figures, the two perpendicular dashed lines at $\xi = -D/2\sigma$ and $\eta = -D/2\sigma$ give the original coordinate axes with the origin O while the two dotted lines intersect at $\overline{O}$. (Both O and $\overline{O}$ are not marked in the figures for neatness.) Obviously, the real interface between the two media is given by $z=0$ or the horizontal dashed line, only below which the flux lines are physically meaningful in our present consideration of the GH effect. The flux lines are so drawn that the cross-sectional density indicates the strength of the Poynting vector. The bold line on the lower left gives

the incident beam axis which, if extrapolated forward, meets both the points O and $\overline{O}$. The bold line on the lower right coincides with the reflected beam axis which, if extrapolated backward, meets only $\overline{O}$. This clearly shows the shift of the beam upon reflection. Note that we have chosen smaller values of $k\sigma$ in both figures to manifest the shift and we see that, in Fig. 3(b), there is a flux line in the upper group passing through the interface; as we shall see in Sec. IV C, this gives interesting closed-loop flux lines when the two media are considered. Note also that the subdominant interference terms in Eq. (49) do not have much effect on the results for a very large $k\sigma$.

B. Second medium ($z \geqslant 0$)

With a real $T(x')$, the Poynting vector in the second medium, obtained from the vector product of Eq. (30) and the complex conjugate of Eq. (35), can be simplified in a similar fashion. The result is, again except for the factor $c^2/8\pi\omega^2$ for the TE state ,

$$\mathbf{S} = |t|_0^2 \; e^{-2\kappa_0 z} \; T(\overline{x}\cos\theta_0)[k\sin\theta_0 \; T(\overline{x}\cos\theta_0)\hat{\mathbf{x}} + \beta \; \dot{T}(\overline{x}\cos\theta_0) \; \hat{\mathbf{z}}], \tag{50}$$

implying always a positive x-direction flow. The Poynting vector for the TM state has again the same form except for the additional ϵ_2 in the denominator. It is then the modification of Eq. (14) for the evanescent wave in the case of a beam. In particular, it implies a negative x direction (or backward) energy flow for a negative dielectric constant (or permittivity). Nontheless, the flux lines always satisfy the same equation which has the following solution:

$$\kappa_0 z = \ln|T(\overline{x}\cos\theta_0)| + \text{const}, \tag{51}$$

where we have made use of Eq. (29). This means that, for a given transverse field profile of the incident beam, the flux lines have the same z vs $\overline{x}$ shape irrespective of any state of wave polarization and any case of the direction of shift, yet the flow direction in the case of negative shift is opposite to that in the case of positive shift.

For a Gaussian beam of the form given by Eq. (43), the solution reduces to

$$\kappa_0 z = -\overline{x^2}\cos^2\theta_0/2\sigma^2 + \text{const} = -\xi^2/2 + \text{const} \tag{52}$$

which, symmetric in $\overline{x}$ as expected, gives parabolic flux lines as shown in Fig. 4(a). Nevertheless, we want to point out that, for a beam profile other than a Gaussian, the flux lines are not at all parabolic. For example, if

$$T(v) = \exp(-v^4/4\sigma^4 + v^3/9\sigma^3 + 2v^2/3\sigma^2] \tag{53}$$

a modulated two-hump profile with two different peaks at $v/\sigma = -1$ and 4/3, and a trough at $v = 0$, the flux lines are given by

$$\kappa_0 z = -\xi^2(\xi^2/4 - \xi/9 - 2/3) + \text{const}. \tag{54}$$

A few typical lines are plotted in Fig. 4(b). This example of a two-hump profile, as we shall see shortly, is useful in understanding the energy flux pattern throughout the region in view of the parity change (or left-right inversion) of the image in reflection. As another example, let us take

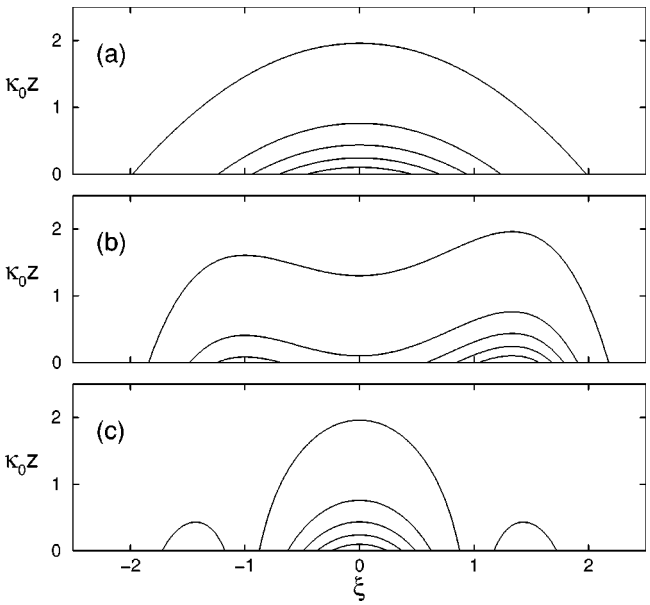

FIG. 4. Three flux patterns in the second medium for three different transverse profiles: (a) Gaussian in Eq. (43), (b) two-hump in Eq. (53), and (c) sinc function in Eq. (55), with the cross-sectional flux line density proportional to the intensity.

$$T(v) = \frac{\sin \pi v/\sigma}{\pi v/\sigma}, \tag{55}$$

a sinc profile resulted from a single-slit diffraction. The flux lines are given by

$$\kappa_0 z = \ln\left|\frac{\sin\pi\xi}{\pi\xi}\right| + \text{const} \tag{56}$$

and a few of them are plotted in Fig. 4(c). In all the three figures, the two ends of every flux line meet the interface. This implies transfer of energy with the first medium. Furthermore, the cross-sectional density of the flux lines indicates the intensity.

C. The two media combined

First, we want to make sure the boundary conditions as stated near the end of Sec. II are properly satisfied. To show this we note that the two components of the Poynting vector in the first medium as given by Eq. (37) can be shown to take the following boundary values from below:

$$S_x(z = 0_-) = 2k\sin\theta_0(1 + \cos\phi_0)[T(\overline{x}\cos\theta_0)]^2, \tag{57}$$

$$S_z(z = 0_-) = 2kD \; \cos^3\theta_0 \; T(\overline{x}\cos\theta_0) \times \dot{T}(\overline{x}\cos\theta_0)/(1 - \epsilon_2/\epsilon_1),$$

where Eqs. (36), (40), and (41) have been used, expansions of the T functions around $\overline{x}\cos\theta_0$ to first order in D (like that at the end of Sec. III) have been made, and terms of second

order have been dropped. Note that S_x is always positive. It is now easy to see that, for the TE state where $\mu=1$, they are exactly equal to the two components in Eq. (50) at $z=0$, where $|t|_0$ and β are, respectively, given by Eq. (28) and Eq. (29). This means that the flux lines do not bend upon crossing the interface. For the TM state, the two components in Eq. (57) have to be divided by ϵ_1 while those in Eq. (50) are divided by ϵ_2 to yield the correct Poynting vector $\mathbf{S}^{(M)}$, say. It is then simple to show the continuity of $\epsilon S_x^{(M)}$ and $S_z^{(M)}$ across the interface, where μ equals ϵ_1/ϵ_2. This means that every flux line has a sudden change of direction upon crossing the interface and there is a discontinuity of the slope. For the case of positive shift, such a change *keeps* the *x* direction of the energy flow while, for the case of negative shift, it *reverses* the *x* direction of the flux lines upon crossing the interface.

With the satisfaction of the boundary conditions, we are now confident to plot the flux lines in the two media. Because the time-averaged Poynting vector is divergence free, the flux pattern in the whole region can be constructed by combining the two graphs separately obtained in Sec. IV A (for $z<0$) and in Sec. IV B (for $z>0$), with the requirement of the continuity of the lines. In particular, if we so combine the two graphs in Figs. 3(b) and 4(a), the closed-loop flux lines around the interface are obviously obtained. To study numerically, we can start with the flux pattern in the first medium calculated according to the equations in Sec. IV A. There are two sets of points of intersection of the flux lines with the interface, one with the lines directed into, and the other with the lines out of, the second medium. We then choose the points in one set as the initial points to draw the flux lines in the second medium according to the solutions in Sec. IV B. The return of these lines to the interface should exactly end at the points in the other set, which can serve as a check of the correctness of our numerical results.

We now show three such patterns throughout the two media in Figs. 5–7, where the two perpendicular dashed (dotted) lines always give the original xz (modified $\xi\eta$-) coordinate axes with the origin O ($\overline{O}$), and the horizontal dashed line always gives the position of the real interface. (Both O and $\overline{O}$ are not marked in the figures for neatness.) Furthermore, all flux lines in these figures are so drawn that its cross-sectional density indicates the intensity.

Figure 5(a) shows the pattern for a Gaussian beam in the TM state with parameters exactly the same as those in Fig. 3(a). As clear from the figure, the flux lines, incident from the lower left, have a part penetrating into the second medium on the left-hand side, keeping close to the surface as the evanescent wave energy flux lines in parabolic shapes afterwards, and re-entering the first medium on the other side. The incident beam axis and the reflected beam axis (indicated by the straight bold lines outside the overlapped region), if extrapolated forward and backward, respectively, can be seen to intersect at the origin $\overline{O}$ of the $\xi\eta$-coordinate system (shown by the two dotted lines) beyond the interface, implying obviously a (positive) shift. Note that the flux lines are denser nearby the interface in the second medium and also that the pattern below the interface is exactly the same as that in Fig. 3(a). For better visualization, Fig. 5(b) gives the pattern near the origin, with tenfold magnification along the η direction. The pattern for a Gaussian beam in the TE state is similar in nature and is therefore not given.

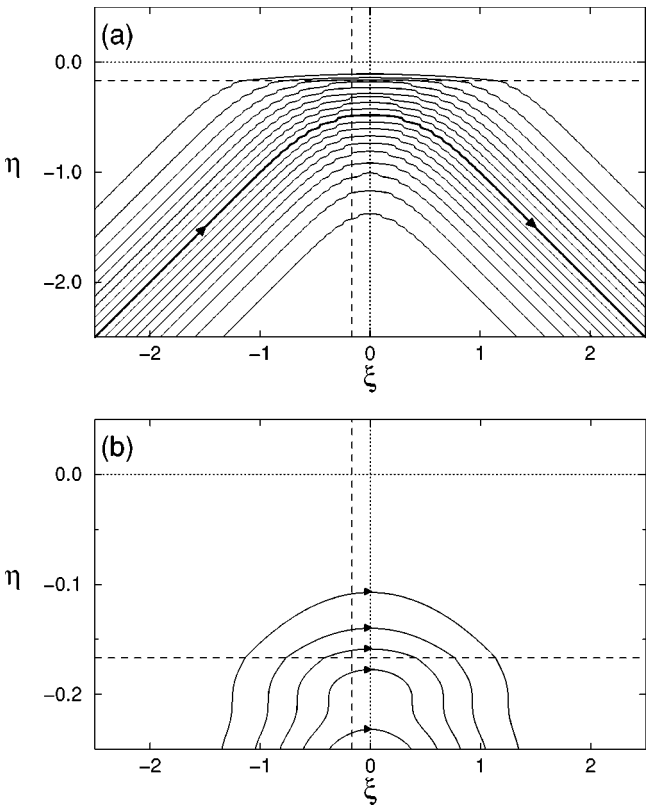

FIG. 5. Flux lines in the two media for a Gaussian beam in the TM state with parameters the same as those in Fig. 3(a). The two perpendicular dashed lines give the original coordinate axes, and the bold line on the lower left in pattern (a) coincides with the incident beam axis. Pattern (b) is a tenfold magnification in η of pattern (a) near the origin.

Figure 6(a) gives the pattern for a Gaussian beam in the TM state with parameters now exactly the same as those in Fig. 3(b). The patterns below the horizontal dashed line in the two figures are therefore exactly the same. This is the case with negative ϵ_2. The intersection of the incident beam axis and the reflected beam axis, again the origin of the $\xi\eta$-coordinate system shown by the dotted lines, now lies in front of the interface and to the left of the original coordinate system (shown by the two dashed lines), indicating a negative shift, albeit a small one. Figure 6(b) is the tenfold magnified pattern (along the vertical direction) of Fig. 6(a) near the origin except that the lines are five times denser. As expected, we see the existence of closed-loop flux lines around the interface. Moreover, we see the incoming flux lines do not pass through the interface at all. Note that these flux lines refer to the flow of energy associated with the *total* field in the absence of dissipation and they do not cross each other. The pattern is therefore the only possible pattern in the case of a negative shift. This also makes sense in view of the existence of a backward energy flow associated with the evanescent wave according to Eq. (14). Note also that the flux lines near the interface are denser in the first medium this time and, moreover, there appears an increasing undulation of intensity when approaching the interface from below along the central line.

Figure 7 gives the pattern for the nonsymmetric two-hump profile in Eq. (53) in the TM-state with parameters exactly the same as those for Fig. 3(a). Besides the positive shift which can be seen by a similar method as that for Fig. 5, we also see how the flux lines come in from the lower left,

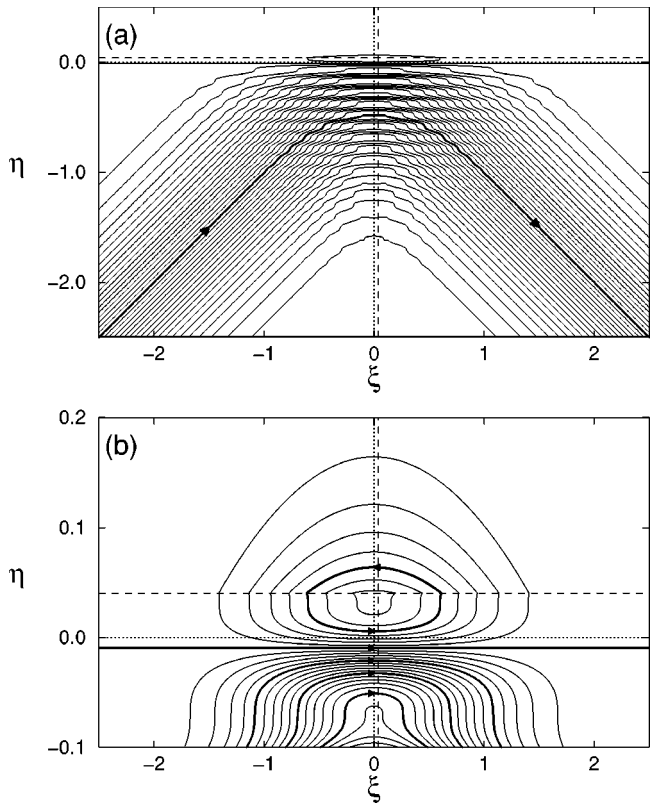

FIG. 6. Flux lines in the two media for a Gaussian beam in the TM state in the case of a negative shift, with parameters the same as those in Fig. 3(b). The horizontal dashed line gives the real interface, and the bold line on the lower left in pattern (a) coincides with the incident beam axis. Pattern (b) is tenfold magnification in η of pattern (a) near the origin, with five times denser lines.

move around with some lines into the second medium and back-and-forth, and finally all go out to the lower right, giving the correct right-left inverted ''image'' in reflection.

V. CONCLUSIONS AND DISCUSSION

In this paper we have calculated the field and the time-averaged Poynting vector everywhere around the interface in the Goos-Hänchen effect in the lowest-order approximation of a good collimated beam. Both the TE (or s) state and the TM (or p) state of polarization and both a positive shift (the usual one) and negative shift are considered. They all satisfy the respective boundary conditions.

For a Gaussian field profile, the energy-flux lines (associated with the evanescent wave) take the shape of parabolas in the second medium, irrespective of the state of the polarization and direction of shift, and the whole flux pattern throughout the two media for each of the two directions of shift has been plotted. While the general features of the pattern for the case of positive shift are expected, we see how

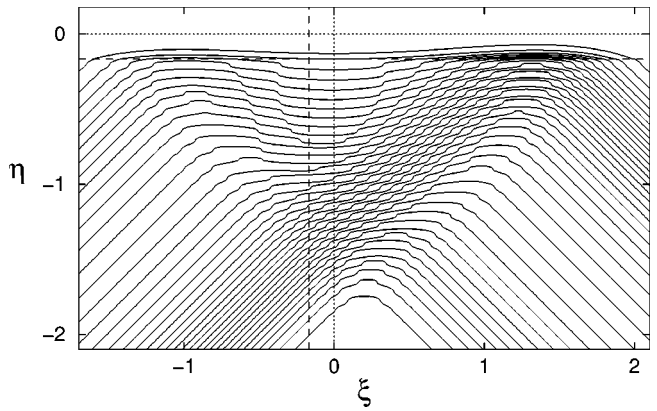

FIG. 7. Flux pattern for the two-hump profile in Eq. (53) in the TM state with parameters same as those in Fig. 3(a). The beam is incident from the lower left and reflected by the interface (horizontal dashed line) to the lower right.

exactly the field energy (associated with the total field) flows throughout the region. For the case of negative shift, we see the interesting closed-loop flux pattern nearby the interface, in addition to the incoming-outgoing flow pattern in the rest of the region. On the other hand, for a non-Gaussian field profile, the flux lines in the second medium are not at all parabolas; they are profile dependent.

It is clear that our calculation simplifies a lot with the assumption of a *real* transverse field profile $T(x')$ of the incident beam in Eq. (21), and this assumption guarantees the paraxial energy flow. On the other hand, we would like to point out that the same simplification still works if T is either (i) a real function multiplied by a complex number or (ii) a complex function with the imaginary part smaller than the real part by at least an order of magnitude. Note that the generally accepted Gaussian beam as given in Eq. (17), under the approximation in Eq. (20), exactly meets the second condition.

Finally, the negative shift, which occurs for a second medium of negative dielectric constant (or permittivity) *and* for the TM state of wave polarization, deserves a few more words. It is well known that a medium of negative permittivity does not support the propagation of a plane wave. Yet it supports an evanescent wave via total reflection and, as clear from Eq. (14), the evanescent wave in the TM state has an energy flow *opposite* to the direction of the phase velocity along the interface. This backward energy flow is in fact the cause of the negative shift. Hence, an experimental detection of a negative shift in total reflection is a demonstration of the existence of a backward flow of energy.

ACKNOWLEDGMENTS

One of the authors (H.M.L.) would like to thank Y. P. Lau of CUHK and Z. Wu of Rutgers University for fruitful discussions.

[1] F. Goos and H. Hänchen, Ann. Phys. (Leipzig) **1**, 333 (1947); **5**, 251 (1949).
[2] K. Artmann, Ann. Phys. (Leipzig) **2**, 87 (1948).
[3] R. H. Renard, J. Opt. Soc. Am. **54**, 1190 (1964).
[4] H. K. V. Lotsch, J. Opt. Soc. Am. **58**, 551 (1968); Optik (Stuttgart) **32**, 116 (1970); **32**, 189 (1970); **32**, 299 (1970); **32**, 553 (1971).
[5] B. R. Horowitz and T. Tamir, J. Opt. Soc. Am. **61**, 586 (1971).

[6] K. W. Chiu and J. J. Quinn, Am. J. Phys. **40**, 1847 (1972).
[7] C. K. Carniglia, J. Opt. Soc. Am. **66**, 1429 (1976); H. K. V. Lotsch, *ibid.* **66**, 1430 (1976).
[8] M. McGuirk and C. K. Carniglia, J. Opt. Soc. Am. **67**, 103 (1977).
[9] H. M. Lai, F. C. Cheng, and W. K. Tang, J. Opt. Soc. Am. A **3**, 550 (1986).
[10] V. Akylas, J. Kaur, and T. M. Knasel, Appl. Opt. **13**, 742 (1974).
[11] J. J. Cowan and B. Anicin, J. Opt. Soc. Am. **67**, 1307 (1977).
[12] D. J. Rhodes and C. K. Carniglia, J. Opt. Soc. Am. **67**, 679 (1977).
[13] K. Chu, J. D. Noble, and T. Y. Chu, Am. J. Phys. **59**, 477 (1991).
[14] F. Bretenaker, A. Le Floch, and L. Dutriaux, Phys. Rev. Lett. **68**, 931 (1992).
[15] T. Tamir and H. L. Bertoni, J. Opt. Soc. Am. **61**, 1397 (1971).
[16] W. J. Wild and C. Lee Giles, Phys. Rev. A **25**, 2099 (1982).
[17] J. Birman, D. N. Pattanayak, and A. Puri, Phys. Rev. Lett. **50**, 1664 (1983).
[18] E. Pfleghaar, A. Marseille, and A. Weis, Phys. Rev. Lett. **70**, 2281 (1993).
[19] B. M. Jost, A-A R. Al-Rashed, and B. E. A. Saleh, Phys. Rev. Lett. **81**, 2233 (1998).
[20] H. Kogelnik and H. P. Weber, J. Opt. Soc. Am. . **64**, 174 (1974)
[21] A. Madrazo and M. Nieto-Veperinas, Opt. Lett. **20**, 2445 (1995).
[22] J. P. Fillard, *Near Field Optics and Nanoscopy* (World Scientific, Singapore, 1996).
[23] B. A. Anicin, R. Fazlic, and M. Kopric, J. Phys. A **11**, 1657 (1978).
[24] M. V. Klein, *Optics* (Wiley, New York, 1970), p. 576.
[25] A. E. Siegman, *An Introduction to Lasers and Masers* (McGraw-Hill, New York, 1971), pp. 304–321.
[26] T. Kojima and Y. Yanagiuchi, J. Appl. Phys. **50**, 41 (1979).